Applied Physics Letters ARTICLE scitation.org/journal/apl

Controlled Si doping of β-Ga_2O_3 by molecular beam epitaxy

Cite as: Appl. Phys. Lett. **121**, 072108 (2022); doi: 10.1063/5.0101132
Submitted: 29 May 2022 · Accepted: 30 July 2022 ·
Published Online: 18 August 2022

View Online Export Citation CrossMark

J. P. McCandless,[1,a] V. Protasenko,[1] B. W. Morell,[2] E. Steinbrunner,[3,4] A. T. Neal,[4] N. Tanen,[2] Y. Cho,[1] T. J. Asel,[4] S. Mou,[4] P. Vogt,[5] H. G. Xing,[1,2,6] and D. Jena[1,2,6]

AFFILIATIONS

[1]School of Electrical and Computer Engineering, Cornell University, Ithaca, New York 14853, USA
[2]Department of Material Science and Engineering, Cornell University, Ithaca, New York 14853, USA
[3]Department of Electrical Engineering, Wright State University, Dayton, Ohio 45435, USA
[4]Air Force Research Laboratory, Materials and Manufacturing Directorate, Wright Patterson AFB, Ohio 45433, USA
[5]Institute of Solid State Physics, University of Bremen, 28359 Bremen, Germany
[6]Kavli Institute at Cornell for Nanoscale Science, Cornell University, Ithaca, New York 14853, USA

[a]**Author to whom correspondence should be addressed:** jpm432@cornell.edu

ABSTRACT

We report controlled silicon doping of Ga_2O_3 grown in plasma-assisted molecular beam epitaxy. Adding an endplate to the Si effusion cell enables the control of the mobile carrier density, leading to over 5-orders of magnitude change in the electrical resistivity. Room temperature mobilities >100 $cm^2/V\,s$ are achieved, with a peak value >125 $cm^2/V\,s$ at a doping density of low-$10^{17}/cm^3$. Temperature-dependent Hall effect measurements exhibit carrier freeze out for samples doped below the Mott criterion. A mobility of 390 $cm^2/V\,s$ is observed at 97 K.

Monoclinic β-Ga_2O_3 has gained much interest in recent years due to its large bandgap ($E_g \sim 4.7$ eV), the availability of large-area substrates, and the ability to increase the conductivity through doping. Donor doping for n-type conductivity has been successfully achieved by metal organic chemical vapor deposition (MOCVD),[1–3] low pressure chemical vapor deposition (LPCVD),[4] metalorganic vapor-phase epitaxy (MOVPE),[5,6] and pulsed laser deposition (PLD).[7] Donor doping of β-Ga_2O_3 with Si, Ge, and Sn atoms has been studied in plasma-assisted (PA) molecular beam epitaxy (MBE)[8–13] as well as with ozone-MBE.[14,15]

In MBE, achieving low carrier densities remains challenging due to the oxidation of the dopant source material in the oxygen-rich MBE environment. This has been observed for Si and Ge.[8,9] Kalarickal *et al.* observed that Si doping in β-Ga_2O_3 is relatively uncontrolled: no change in donor density was observed upon changing the dopant effusion cell temperature.[8] The Si effusion cell temperature (T_{Si}) was changed from 1000 to 800 °C, while the Si density in the film remained stable at $\sim 6 \times 10^{18}/cm^3$. As T_{Si} was lowered to 750 °C, the carrier density dropped to $4.5 \times 10^{17}/cm^3$. They also observe a delta-like doping profile. The Si density shows a clear peak upon opening the Si source shutter, but then it decays—preventing uniform Si doping within an epitaxial layer. They report an unintentional background doping density of $\sim 5 \times 10^{16}/cm^3$.

To explain this behavior, they invoke "active" and "passive" oxidation—terms originating in the study of the oxidation of Si wafers, in 1958, by Wagner.[16] Active oxidation refers to the Si surface being responsive when exposed to O_2—with the Si layer being etched through the formation of the volatile, sub-oxide SiO. This is contrasted with passive oxidation where etching does not occur due to the surface being passivated with SiO_2.[16,17]

Kalarickal *et al.* propose that when O is present in the MBE chamber, O is adsorbed onto the Si surface. Depending on the growth conditions (i.e., the O partial pressure experienced within the Si effusion cell and T_{Si}), active or passive oxidation can occur. Under active oxidation, the volatile, sub-oxide SiO is formed on the Si surface. SiO is then desorbed from the Si surface and incorporates into the film. Under passive oxidation, the SiO is further oxidized to SiO_2 at which point doping ceases. The delta-like doping behavior they believe is due to instability of the active oxidation process and after prolonged periods of time, the SiO fully oxidizes to SiO_2, and the Si profile in the film goes to the background level.

The work of Asel *et al.* reports a higher unintentional doping density than Kalarickal *et al.* and reports this unintentional Si doping is strongly affected by the O plasma power.[18] At $T_{Si} = 900$ °C, the Si background density is $2 \times 10^{18}/cm^3$. The silicon cell shutter was

opened for 2 s to investigate delta doping, and the density increased to $5.3 \times 10^{18}/\text{cm}^3$. Next, they grew two samples in, they believe, the passive oxidation regime with $T_{Si} = 600$ and 300 °C. For both samples, they report the Si density is $\sim 3 \times 10^{17}/\text{cm}^3$, when the shutter is closed. They were able to reduce the carrier density by lowering the plasma power. When the power was lowered from 300 to 250 W, the Si density decreased to $1 \times 10^{16}/\text{cm}^3$. The authors suggest that some of the unintentional doping within the film comes from the quartz plasma tube.

To date, the intentional Si doping density in conventional MBE has been in the high-$10^{18}/\text{cm}^3$. To address this, we investigated a modified effusion cell design. All samples were grown on 5×5 mm^2 or 10×10 mm^2, Fe-doped, semi-insulating, bulk Ga_2O_3 substrates in the (010) orientation. The samples were cleaned with a standard solvent process before being loaded into a Veeco GEN 930 plasma-assisted (PA) MBE system. They were heated to 900 °C, *in situ* and under vacuum (10^{-9} Torr), for 30 min to desorb chemical impurities. A ~250 nm, unintentionally doped (UID), β-Ga_2O_3 buffer layer was grown (unless stated otherwise) to spatially separate the Si doped layers from the Fe tail, which arose due to surface riding effects.[19] Since Fe is a deep acceptor, it compensates the free carriers. Within the Si doped layer, the Fe density is at the detection limit, $\sim 10^{15}/\text{cm}^3$. The surface roughness was measured by atomic force microscopy. X-ray diffraction, aligned to the 020 peak with a symmetric $2\theta - \omega$ scan, revealed no additional peaks, indicating that the samples were phase-pure.

Control samples were grown with a conventional Si effusion cell with a conical crucible. Test samples were grown where an endplate was inserted into the opening of the Si crucible (i.e., a modified source), as shown in Fig. 1. A similar approach has been used in the past to improve flux stability of Sr in an oxide MBE system.[20] A pyrolytic boron nitride (PBN) endplate was used with 350 holes drilled into the surface, each of diameter 0.203 mm. The holes are drilled at an angle, the holes are 10 degrees normal to the surface. The endplate is oriented such that the holes are pointed toward the MBE chamber wall, rather than directly at the sample, in an effort to reduce the SiO_x flux experienced by the film. Using this modified effusion cell, Si doping concentrations ranging from $\sim 1 \times 10^{17}$ to $\sim 1 \times 10^{20}/\text{cm}^3$ were achieved in epitaxial β-Ga_2O_3 as T_{Si} was varied from 890 to 1100 °C.

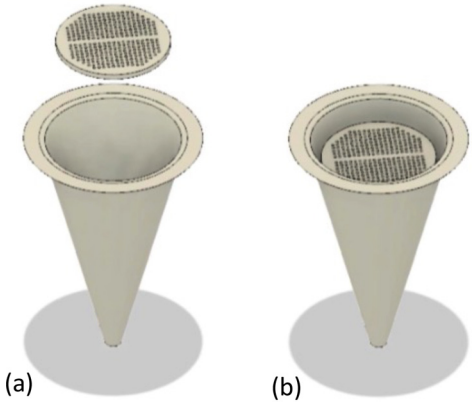

FIG. 1. (a) A PBN endplate with holes is (b) inserted into the orifice of the Si crucible—affecting the O partial pressure experienced by the Si material.

Figure 2 shows the silicon density profiles obtained from secondary ion mass spectrometry (SIMS). All the Ga_2O_3 samples in this figure are grown with a Ga flux of 1.1 atoms/nm^2 s and an O flux of 2.0 atoms/nm^2 s. Figure 2(a) shows SIMS data obtained using the conventional Si dopant source. Comparing 1050 and 1000 °C, a change from 1.5 to $1.2 \times 10^{20}/\text{cm}^3$ is observed. At 950 °C, a lower concentration ($\sim 4 \times 10^{19}/\text{cm}^3$) is achieved, but a peak rather than a plateau is observed, and below $T_{Si} = 950$ °C, intentional doping is indistinguishable from the background. This can be understood in the context of passive and active oxidation. Below $T_{Si} = 950$ °C, SiO_2 formation on the Si source surface (i.e., passive oxidation) hinders the desorption and incorporation of the dopant, as indicated by Kalarickal *et al.* As T_{Si} heats to 950 °C, the source undergoes a disproportionation reaction, resulting in SiO on the surface. The SiO is then desorbed and incorporates into the β-Ga_2O_3 film.

Figure 2(b) shows the SIMS profile obtained using the modified Si effusion cell. The substrate growth temperature, measured using a pyrometer pointed at the substrate, was $T_{sub} \sim 515$ °C. The O_2 flow rate for all samples is 1.4 sccm, which results in a chamber pressure of $2.5 - 3.2 \times 10^{-5}$ Torr. A ~150 nm undoped buffer layer was grown, followed by alternating 1 h layers of UID and intentionally doped Ga_2O_3 layers. T_{Si} was increased in 100 °C steps. SIMS indicates that the Si concentration was at the background level, while the effusion

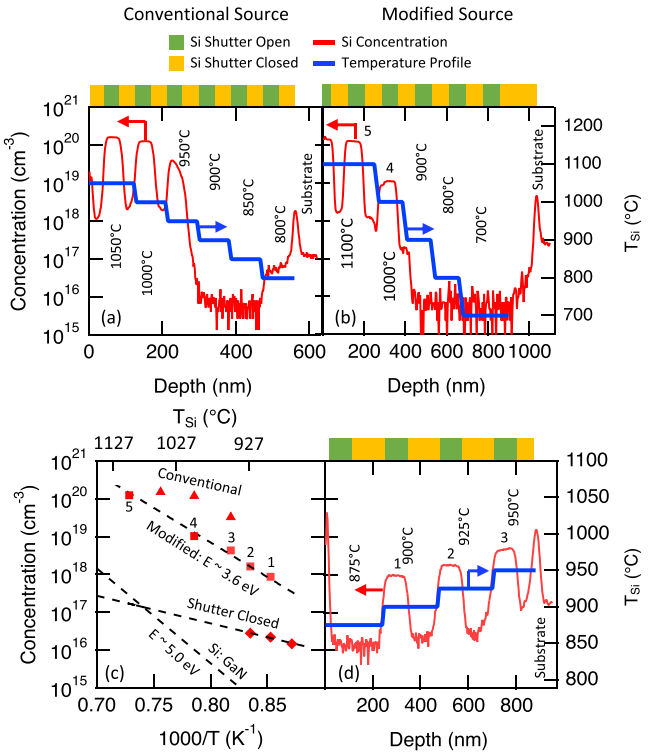

FIG. 2. Stacks of Ga_2O_3 layers were grown with alternating doped and non-doped layers. The impurity levels were measured through SIMS. (a) The Si profile obtained by SIMS of a stack doped by a conventional source. (b) and (d) Doped stacks through the use of a modified source. (c) The extracted data from the three SIMS stacks shown, along with SIMS from a Si doped GaN stack as reference. Additionally, activation energies are extracted.

cell was heated from 700 to 900 °C. As T_{Si} was increased from 900 to 1000 °C with the shutter closed, a jump is observed in the Si concentration with a shoulder at $\sim 2 \times 10^{17}/cm^3$. At $T_{Si} = 1000$ and 1100 °C, clear steps are observed as the Si concentration is increased from 10^{19} to $10^{20}/cm^3$.

To further understand the Si doping behavior around $T_{Si} = 900$ °C, an additional SIMS stack was grown, with the Si profile shown in Fig. 2(d). A 0.5 h UID buffer layer was grown, followed by alternating layers of doped and UID Ga_2O_3. To clearly demarcate the doping density in the film when the source shutter is closed, the doped layers were grown for 1 h, while the UID layers were grown for 1.5 h. T_{Si} was stepped down from 950 to 875 °C in 25 °C steps.

Figure 2(d) indicates a Si doping plateau at 900 °C in contrast with Fig. 2(b). This is likely due to passive oxidation of the Si in the latter case. In Fig. 2(b), the O plasma source was ignited when the Si effusion cell was at 700 °C. At this temperature, the silicon source was exposed to active oxygen for 7.2 h during the growth of the buffer layer and the alternating UID/doped layers until, finally, the effusion cell was heated from 900 to 1000 °C. Before this T_{Si} increase, SiO_2 was formed on the Si surface, preventing SiO desorption, resulting in Si being at the background level within the film. When T_{Si} was finally heated up from 900 °C, the source material underwent a disproportionation reaction, changing from passive to active oxidation. In Fig. 2(d), the source material was always in the active oxidation state—enabling doping at 900 °C. This raises the question of whether it was the long exposure time of the Si source to the O plasma that caused it to enter the passive oxidation regime, or if it was the doping source temperature at the time the O plasma was struck. It is likely the latter. For when the O plasma is struck and the effusion cell is at 890 °C, SIMS indicates uniform doping densities after 5.5 h of active O exposure (shown later in Fig. 4).

Figure 2(c) plots the measured, average doping concentration as a function of $1000/T_{Si}$ for the data shown in Fig. 2(a), shown by triangles, and Figs. 2(b) and 2(d) shown by squares. The diamonds are the extracted carrier densities obtained from Fig. 2(d) when the effusion cell shutter is closed. As T_{Si} is changed, an activation energy of ~3.6 eV is observed for the modified source, which is greater than what is observed for the conventional source. This activation energy is in good agreement with the theoretical SiO activation energy of 3.57 eV and lends support to the hypothesis proposed by Kalarickal *et al.*[21] In contrast, the dashed line labeled Si:GaN captures the SIMS data from Faria *et al.* for Si doped GaN—providing a reference for Si not affected by source oxidation.[22]

The silicon activation energy obtained when the doping source shutter is closed (red diamonds) is based on $T_{Si} = 875$, 900, and 925 °C data from Fig. 2(d). When the shutter is closed for the other temperatures in Figs. 2(a), 2(b), and 2(d), the Si profile, instead of being constant, has a Si density, which reaches a minimum at a point. This is likely due to Si diffusion from the doped region into the undoped region. As such, the observed values do not necessarily represent the true UID Si concentration.

It is worth observing that the background doping obtained when the shutter is closed is acceptable if the desired doping densities are low-10^{18} and $10^{17}/cm^3$. This will result in background densities in the mid to low-$10^{16}/cm^3$. If, however, higher doping densities are desired, the background doping level will also rise. For example, for intentional doping densities in the mid-$10^{19}/cm^3$, the background density would likely be $\sim 1 \times 10^{17}/cm^3$. This increase in background doping may be due to SiO leaking from around the shutter, or from SiO_x desorption from the shutter blade. Further investigation is needed to verify this hypothesis. If higher doping densities are needed, a growth interrupt while the effusion cell temperature is changed is necessary.

Next, a series of uniformly doped samples were grown so Hall effect measurements could be performed to evaluate the transport properties of Si-doped β-Ga_2O_3. The critical Mott donor density (n_c) above which a semiconductor exhibits metallic conductivity is $n_c = 0.26\, a_0^{-3}$ where $a_0 = 1.93$ nm is the effective Bohr radius.[23,24] For Ga_2O_3, $n_c \sim 2.4 \times 10^{18}/cm^3$. Three samples with free carrier densities below the Mott transistion were selected for temperature dependent Hall effect measurements in a Lakeshore Hall system with a 1 T magnet. The temperature was varied from 300 K down to 20 K.

The measured 300 K resistivities are shown for samples doped with the conventional source and for samples doped with the modified source in Figs. 3(a) and 3(b), respectively. With the conventional source, it is difficult to obtain consistent doping; several samples in the series which were too resistive to measure are not shown. In contrast, samples doped with the modified source clearly show the desired increase in conductivity as T_{Si} is increased. The resistivity changes by 5 orders of magnitude, from 149 Ω cm at $T_{Si} = 865$ °C to 2.67×10^{-3} Ω cm at $T_{Si} = 1050$ °C. Note: not all data in this plot are grown with same Ga flux or T_{sub}. The Ga flux was increased to increase the growth rate, and the T_{sub} was adjusted to reduce the surface roughness.

From Fig. 3(b), three samples were selected for temperature dependent Hall effect measurements. The growth conditions are listed in Table I. The growth conditions for samples 1 and 3 were the same as those used previously for the SIMS stacks shown in Fig. 2. The growth rate was ~93 nm/h. Sample 2 was grown with the same Ga to O flux ratio as samples 1 and 3, but with lower absolute flux values. The growth rate for sample 2 was ~60 nm/h.

Table I summarizes the growth conditions and transport properties of the three samples. All three samples show carrier freeze out at low temperature, as seen in Fig. 4(a), indicating the doping density is below the Mott criterion. SIMS doping profiles of these three samples

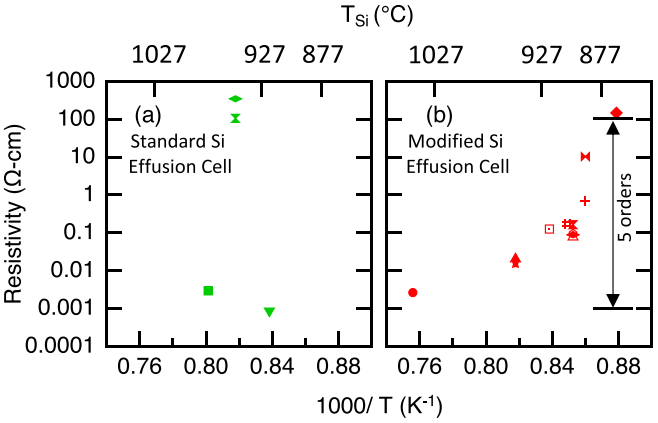

FIG. 3. Resistivity is plotted vs the effusion cell temperature for (a) samples grown with a conventional Si source, and for (b) samples grown with the modified source. It is clear that as the Si flux is reduced, with decreasing source temperature, the resistivity increases.

TABLE I. The Ga flux, O flux, and growth temperature (T_{sub}) are listed for three samples, which were studied with temperature dependent Hall, along with a summary of the Hall effect data. The doping effusion cell temperature, T_{Si}, is listened for each sample along with the Si density from SIMS (N_D), the calculated (n_{calc}) and measured free carrier density (n_{RT}), and the carrier mobility (μ_{RT}) at room temperature. Additionally, the peak mobility (μ_{max}) is listed along with the corresponding carrier density and measurement temperature. Activation energy is also reported.

Sample number	Ga flux atoms/nm^{2}s	O flux, atoms/nm^{2}s	T_{sub}, °C	T_{Si}, °C	N_D, cm^{-3}	n_{calc}, cm^{-3}	n_{RT}, cm^{-3}	μ_{RT}, cm^2/V s	T_{max}, K	n_{max}, cm^{-3}	μ_{max}, cm^2/V s	E_a, meV
1	1.1	2.0	523	900	1.30×10^{18}	7.80×10^{17}	8.16×10^{17}	107.4	115	4.09×10^{17}	219.9	15.3
2	0.7	1.4	502	905	1.09×10^{18}	6.79×10^{17}	4.38×10^{17}	87.5	110	1.88×10^{17}	189.6	41.9
3	1.1	2.0	523	890	1.4×10^{17}	1.22×10^{17}	1.11×10^{17}	128.6	97	2.44×10^{16}	390.2	33.4

are shown in Fig. 4(b). The donor densities N_D obtained from SIMS are listed in Table I. The SIMS profiles indicate that uniform doping was achieved despite the effusion cell being exposed to O for 5.5 h, as mentioned previously.

Table I lists the donor activation energies extracted by fitting the carrier density, from the Arrhenius plot in Fig. 4(c), with the charge neutrality equation, $N_D^+ + p = N_A^- + n$. In Fig. 4(d), a comparison is made of activation energies of these three samples, along with reported values from the literature for non-MBE growth methods.[1,2,4,25,26] The activation energies reported here range from 15.3 to 41.9 meV. The lowest doped sample offers the most reliable measure of the donor activation energy. As the doping density increases, the impurity state energy levels spread and form an impurity band, resulting in decreased activation energies at increased doping densities. The activation energy of sample 3 is 33.4 meV, where $N_D = 1.40\times10^{17}/\text{cm}^3$ and $N_A = 2.59\times10^{15}/\text{cm}^3$. The activation energy is in good agreement with the values from literature.

Figure 4(e) shows the measured Hall effect mobilities for each of the three sample as a function of temperature. Samples 2 and 3 display RT electron mobilities over 100 cm^2/Vs. The peak RT mobility was ~129 cm^2/Vs with a corresponding doping density of 1.07×10^{17} cm^{-3}. All samples demonstrate a mobility enhancement as the temperature decreases to 100 K due to the reduction in the polar optical phonon scattering rate. The peak mobility among the three samples was ~390 cm^2/Vs at a temperature of 97 K and a free carrier density of $2.44\times10^{16}/\text{cm}^3$.

Control samples were grown without Si doping under the same growth conditions as used for samples 1 and 3 in Table I. The resistivities of these samples were very high, indicating that with the same growth conditions, we can achieve low-carrier densities and high mobilities as well as insulating films.

In Fig. 5, we benchmark the measured transport properties obtained in this work with values reported in the literature for various growth techniques and with various dopants. Figure 5(a) provides an overview, showing the mobilities vs carrier densities reported for many growth techniques and for Si, Ge, and Sn dopants. Figures 5(b) and 5(c), in addition to plotting mobility vs carrier density values from Fig. 5(a), show the calculated mobility limit (TOT), along with the limiting scattering mechanisms—ionized impurities (II) and polar optical phonons (PO). Figure 5(b) shows data reported only by MBE variants. In addition to conventional PA-MBE and ozone-MBE, another approach that has been explored is metal oxide catalyzed epitaxy (MOCATAXY). MOCATAXY involves the addition of In which serves as a catalyst.[27,28] With this technique, low density doping was achieved with Sn.[13] Densities as low as $3.9\times10^{16}/\text{cm}^3$ were reported, which resulted in a mobility of 136 cm^2/V s at RT. A second approach is to use a sub-oxide source.[15,29] Vogt *et al.* report controllable doping through the use of a SnO source, instead of a Sn source.[15]

Finally, Fig. 5(c) shows the MBE data presented here, along with Si doping for non-MBE growth techniques. From this, it is clear that the approach outlined here can achieve excellent room temperature mobilities at fixed densities, comparable with other growth techniques. Additionally, it is possible to grow thin, single/few layer heterostructures with sharp interfaces by MBE, which is beneficial for the formation of quantized heterostructures.

In the future, the impact of the endplate design for the dopant effusion cell should be studied further with an emphasis toward reducing the background doping at high effusion cell temperatures.

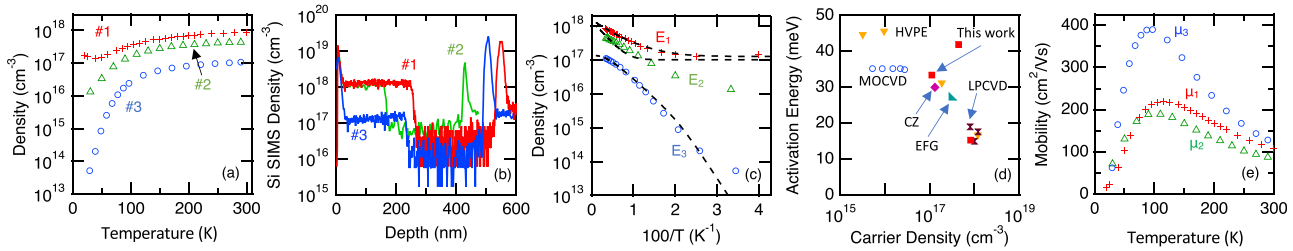

FIG. 4. Temperature dependent Hall effect measurement data are shown for three samples. (a) The carrier density is plotted as a function of temperature. Each sample shows carrier freeze out with decreasing temperature. (b) The SIMS data for the three samples. Each sample displays uniform doping. (c) The density vs inverse temperature from which an activation energy can be extracted. (d) The extracted activation energies for these samples, along with values reported in the literature. (e) A plot of the mobility vs temperature. A mobility enhancement is observed due to a reduction in the polar optical phonon scattering rate as the temperatures are decreased from room temperature.

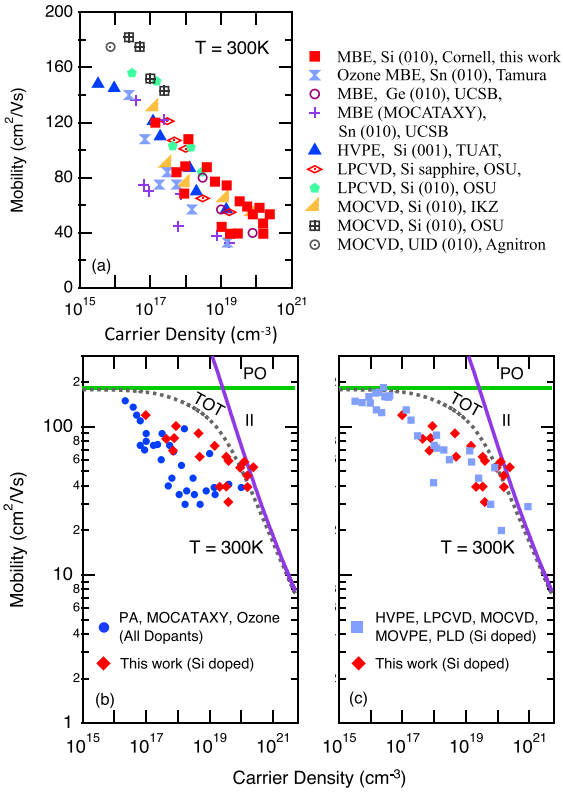

FIG. 5. The growths reported here are bench marked against other reports of Ga_2O_3 doping. (a) The reported mobilities vs carrier density for different growth techniques and for different dopants for various orientations and various substrate orientations. (b) and (c) The mobility vs free carrier concentration is plotted along with the scattering mechanisms—ionized impurities (II), polar optical phonons (PO), and the total mobility (TOT) are shown. (b) Results by MBE, regardless of dopant, while (c) shows the data for Si dopants for non-MBE growth techniques.

There are likely two principles that allow these doping improvements. First, by inserting the endplate, there is likely an increase in pressure within the effusion cell due to the reduced cross-sectional opening and reduced crucible volume. This results in a shift in the equilibrium pressure within the dopant crucible, reducing the O partial pressure experienced within the Si crucible. This will have the effect of lowering the minimum T_{Si} under which active oxidation occurs for a fixed growth chamber O partial pressure. Second, there is likely a reduction in the doping density due to the reduction in the effective cross-sectional area of the crucible for a fixed T_{Si} and fixed O partial pressure. These qualitative working-hypotheses and the contributions from each of the aforementioned mechanisms need to be explored quantitatively in the future.

Moreover, the hypothesis that multi-order doping density control achieved here is due to SiO and is bolstered by the fact that the activation energy obtained from the SIMS in Fig. 2 is in good agreement with the theoretical SiO value.[21] In the future, a study employing a residual gas analyzer and quadrupole mass spectrometer should be performed to further understand the chemical species emitted from the dopant effusion cell with and without the end plate.

In summary, we demonstrate that using an effusion cell with an endplate enables the control of the silicon donor density in β-Ga_2O_3. Carrier densities from low-$10^{17}/cm^3$ to low-$10^{20}/cm^3$ display high room temperature electron mobilities and are comparable with values reported in the literature for comparable doping densities. With better understanding and more optimization of the endplate design, even lower controlled doping densities should be achievable in the future.

This research is supported by the Air Force Research Laboratory-Cornell Center for Epitaxial Solutions (ACCESS), monitored by Dr. Ali Sayir (No. FA9550-18-1-0529). J.P.M. acknowledges the support of a National Science Foundation Graduate Research Fellowship under Grant No. DGE'2139899. B.W.M. acknowledges ELI Student Grant. This work uses the CCMR and CESI Shared Facilities partly sponsored by the NSF MRSEC program (No. DMR-1719875) and No. MRI DMR-1338010, and the Kavli Institute at Cornell (KIC).

AUTHOR DECLARATIONS

Conflict of Interest

The authors have no conflicts to disclose.

Author Contributions

Jonathan McCandless: Conceptualization (equal); Data curation (lead); Formal analysis (lead); Investigation (lead); Visualization (lead); Writing – original draft (lead); Writing – review and editing (equal). **Patrick Vogt:** Formal analysis (supporting); Investigation (supporting); Writing – review and editing (supporting). **Huili Grace Xing:** Formal analysis (supporting); Funding acquisition (equal); Methodology (equal); Resources (equal); Writing – review and editing (supporting). **Debdeep Jena:** Conceptualization (supporting); Formal analysis (equal); Funding acquisition (equal); Methodology (equal); Resources (equal); Supervision (equal); Writing – original draft (supporting); Writing – review and editing (equal). **Vladimir Protasenko:** Conceptualization (equal); Formal analysis (equal); Writing – review and editing (supporting). **Brad Morell:** Formal analysis (supporting); Investigation (supporting). **Erich Steinbrunner:** Formal analysis (supporting); Investigation (supporting). **Adam T Neal:** Formal analysis (supporting); Investigation (supporting). **Nicholas Tanen:** Conceptualization (equal); Investigation (supporting). **Yong Jin Cho:** Conceptualization (equal). **Thaddeus J Asel:** Validation (supporting). **Shin Mou:** Supervision (supporting); Writing – review and editing (supporting).

DATA AVAILABILITY

The data that support the findings of this study are available from the corresponding author upon reasonable request.

REFERENCES

[1]F. Alema, Y. Zhang, A. Osinsky, N. Valente, A. Mauze, T. Itoh, and J. S. Speck, "Low temperature electron mobility exceeding 104 cm^2/V s in MOCVD grown β-Ga_2O_3," APL Mater. **7**, 121110 (2019).

[2]Z. Feng, A. F. Anhar Uddin Bhuiyan, M. R. Karim, and H. Zhao, "MOCVD homoepitaxy of Si-doped (010) β-Ga_2O_3 thin films with superior transport properties," Appl. Phys. Lett. **114**, 250601 (2019).

[3]Y. Zhang, F. Alema, A. Mauze, O. S. Koksaldi, R. Miller, A. Osinsky, and J. S. Speck, "MOCVD grown epitaxial β-Ga_2O_3 thin film with an electron mobility of 176 cm^2/V s at room temperature," APL Mater. **7**, 022506 (2019).

[4]S. Rafique, M. R. Karim, J. M. Johnson, J. Hwang, and H. Zhao, "LPCVD homoepitaxy of Si doped β-Ga_2O_3 thin films on (010) and (001) substrates," Appl. Phys. Lett. **112**, 052104 (2018).
[5]M. Baldini, M. Albrecht, A. Fiedler, K. Irmscher, D. Klimm, R. Schewski, and G. Wagner, "Semiconducting Sn-doped β-Ga_2O_3 homoepitaxial layers grown by metal organic vapour-phase epitaxy," J. Mater. Sci. **51**, 3650–3656 (2016).
[6]M. Baldini, M. Albrecht, A. Fiedler, K. Irmscher, R. Schewski, and G. Wagner, "Si- and Sn-doped homoepitaxial β-Ga_2O_3 layers grown by MOVPE on (010)-oriented substrates," ECS J. Solid State Sci. Technol. **6**, Q3040 (2017).
[7]K. D. Leedy, K. D. Chabak, V. Vasilyev, D. C. Look, J. J. Boeckl, J. L. Brown, S. E. Tetlak, A. J. Green, N. A. Moser, A. Crespo, D. B. Thomson, R. C. Fitch, J. P. McCandless, and G. H. Jessen, "Highly conductive homoepitaxial Si-doped Ga_2O_3 films on (010) β-Ga_2O_3 by pulsed laser deposition," Appl. Phys. Lett. **111**, 012103 (2017).
[8]N. K. Kalarickal, Z. Xia, J. McGlone, S. Krishnamoorthy, W. Moore, M. Brenner, A. R. Arehart, S. A. Ringel, and S. Rajan, "Mechanism of Si doping in plasma assisted MBE growth of β-Ga_2O_3," Appl. Phys. Lett. **115**, 152106 (2019).
[9]E. Ahmadi, O. S. Koksaldi, S. W. Kaun, Y. Oshima, D. B. Short, U. K. Mishra, and J. S. Speck, "Ge doping of β-Ga_2O_3 films grown by plasma-assisted molecular beam epitaxy," Appl. Phys. Express **10**, 041102 (2017).
[10]N. Moser, J. McCandless, A. Crespo, K. Leedy, A. Green, A. Neal, S. Mou, E. Ahmadi, J. Speck, K. Chabak, N. Peixoto, and G. Jessen, "Ge-doped β-Ga_2O_3 MOSFETs," IEEE Electron Device Lett. **38**, 775–778 (2017).
[11]H. Okumura, M. Kita, K. Sasaki, A. Kuramata, M. Higashiwaki, and J. S. Speck, "Systematic investigation of the growth rate of β-Ga_2O_3 (010) by plasma-assisted molecular beam epitaxy," Appl. Phys. Express **7**, 095501 (2014).
[12]S.-H. Han, A. Mauze, E. Ahmadi, T. Mates, Y. Oshima, and J. S. Speck, "n-type dopants in (001) β-Ga_2O_3 grown on (001) β-Ga_2O_3 substrates by plasma-assisted molecular beam epitaxy," Semicond. Sci. Technol. **33**, 045001 (2018).
[13]A. Mauze, Y. Zhang, T. Itoh, E. Ahmadi, and J. S. Speck, "Sn doping of (010) β-Ga_2O_3 films grown by plasma-assisted molecular beam epitaxy," Appl. Phys. Lett. **117**, 222102 (2020).
[14]K. Sasaki, A. Kuramata, T. Masui, G. Villora, K. Shimamura, and S. Yamakoshi, "Device-quality β-Ga_2O_3 epitaxial films fabricated by ozone molecular beam epitaxy," Appl. Phys. Express **5**, 035502 (2012).
[15]P. Vogt, F. V. Hensling, K. Azizie, C. S. Chang, D. Turner, J. Park, J. P. McCandless, H. Paik, B. J. Bocklund, G. Hoffman, O. Bierwagen, D. Jena, H. G. Xing, S. Mou, D. A. Muller, S. L. Shang, Z. K. Liu, and D. G. Schlom, "Adsorption-controlled growth of Ga_2O_3 by suboxide molecular-beam epitaxy," APL Mater. **9**, 031101 (2021).
[16]C. Wagner, "Passivity during the oxidation of silicon at elevated temperatures," J. Appl. Phys. **29**, 1295–1297 (1958).
[17]F. W. Smith and G. Ghidini, "Reaction of oxygen with Si(111) and (100): Critical conditions for the growth of SiO_2," J. Electrochem. Soc. **129**, 1300–1306 (1982).
[18]T. J. Asel, E. Steinbrunner, J. Hendricks, A. T. Neal, and S. Mou, "Reduction of unintentional Si doping in β-Ga_2O_3 grown via plasma-assisted molecular beam epitaxy," J. Vac. Sci. Technol. A **38**, 043403 (2020).
[19]A. Mauze, Y. Zhang, T. Mates, and J. Speck, "Investigation of Fe incorporation in (010) β-Ga_2O_3 films grown by plasma-assisted molecular beam epitaxy," in *2019 Compound Semiconductor Week (CSW)* (IEEE, 2019), p. 1-1, abstract available at https://ieeexplore.ieee.org/document/8819314
[20]Y. S. Kim, N. Bansal, C. Chaparro, H. Gross, and S. Oh, "Sr flux stability against oxidation in oxide-molecular-beam-epitaxy environment: Flux, geometry, and pressure dependence," J. Vac. Sci. Technol. A **28**, 271–276 (2010).
[21]K. M. Adkison, S. L. Shang, B. J. Bocklund, D. Klimm, D. G. Schlom, and Z. K. Liu, "Suitability of binary oxides for molecular-beam epitaxy source materials: A comprehensive thermodynamic analysis," APL Mater. **8**, 081110 (2020).
[22]F. A. Faria, J. Guo, P. Zhao, G. Li, P. K. Kandaswamy, M. Wistey, H. Xing, and D. Jena, "Ultra-low resistance ohmic contacts to GaN with high Si doping concentrations grown by molecular beam epitaxy," Appl. Phys. Lett. **101**, 032109 (2012).
[23]N. F. Mott, "Metal-insulator transitions," Rev. Mod. Phys. **40**, 677–683 (1968).
[24]P. P. Edwards and M. J. Sienko, "Universality aspects of the metal-nonmetal transition in condensed media," Phys. Rev. B **17**, 2575–2581 (1978).
[25]A. T. Neal, S. Mou, S. Rafique, H. Zhao, E. Ahmadi, J. S. Speck, K. T. Stevens, J. D. Blevins, D. B. Thomson, N. Moser, K. D. Chabak, and G. H. Jessen, "Donors and deep acceptors in β-Ga_2O_3," Appl. Phys. Lett. **113**, 062101 (2018).
[26]K. Goto, K. Konishi, H. Murakami, Y. Kumagai, B. Monemar, M. Higashiwaki, A. Kuramata, and S. Yamakoshi, "Halide vapor phase epitaxy of Si doped β-Ga_2O_3 and its electrical properties," Thin Solid Films **666**, 182–184 (2018).
[27]P. Vogt, A. Mauze, F. Wu, B. Bonef, and J. S. Speck, "Metal-oxide catalyzed epitaxy (MOCATAXY): The example of the O plasma-assisted molecular beam epitaxy of β-$(Al,Ga)_2O_3$/β-Ga_2O_3 heterostructures," Appl. Phys. Express **11**, 115503 (2018).
[28]P. Vogt, O. Brandt, H. Riechert, J. Lahnemann, and O. Bierwagen, "Metal-exchange catalysis in the growth of sesquioxides: Towards heterostructures of transparent oxide semiconductors," Phys. Rev. Lett. **119**, 196001 (2017).
[29]P. Vogt, F. V. Hensling, K. Azizie, J. P. McCandless, J. Park, K. DeLello, D. A. Muller, H. G. Xing, D. Jena, and D. G. Schlom, "Extending the kinetic and thermodynamic limits of molecular-beam epitaxy utilizing suboxide sources or metal-oxide-catalyzed epitaxy," Phys. Rev. Appl. **17**, 034021 (2022).